Flat-surface, step-edge, facet–facet, and facet–step diffusion barriers in growth of a Pb mesa

Yong Han [a,*], Guang-Hong Lu [b], Byeong-Joo Lee [c], Feng Liu [a]

[a] Department of Materials Science and Engineering, University of Utah, Salt Lake City, UT 84112, United States
[b] Department of Physics, Beijing University of Aeronautics and Astronautics, Beijing 100083, China
[c] Department of Materials Science and Engineering, Pohang University of Science and Technology, Pohang 790-784, Republic of Korea

ARTICLE INFO

ABSTRACT

We obtain important energy parameters for understanding growth kinetics of a faceted Pb mesa. Specifically, extensive calculations of diffusion barriers are performed for a Pb adatom: (i) on a flat Pb(1 1 1) or Pb(0 0 1) surface; (ii) crossing a single A- or B-step edge on Pb(1 1 1) surface; (iii) crossing a facet–facet edge between Pb(1 1 1) facet and Pb(0 0 1) facet, or between Pb(1 1 1) facet and Pb(1 1 1̄) facet; (iv) crossing a facet–step joint between Pb(0 0 1) facet and A-step, or between Pb(1 1 1̄) facet and B-step, using a modified embedded atom method. We investigate two different diffusion modes: direct hopping of an adatom, and exchange mechanism between an adatom and substrate atom(s). Direct hopping diffusion is more favorable over exchange mechanism for an adatom on a flat (1 1 1) or (0 0 1) surface. Diffusion crossing A-step edge favors direct hopping, while diffusion crossing B-step edge favors exchange mechanism. For facet–facet or facet–step diffusion, the exchange mechanism is always favorable over direct hopping. The diffusion barriers obtained here have been used to reasonably explain the intriguing kinetic growth of a Pb mesa in recent experiments. In addition, we also discuss low-index planes of Pb[1̄10] crystallographic zone related to the choices of sidewalls in the formation of a Pb mesa by calculating corresponding surface free energies.

© 2008 Elsevier B.V. All rights reserved.

1. Introduction

The key kinetic energy parameters controlling epitaxial growth of multilayer films or islands are the diffusion barriers, including the flat-surface diffusion barrier and the step-edge barrier. The flat-surface diffusion barrier is defined as the energy difference between energy minimum and saddle point on the minimum energy path (MEP) of diffusion when an adatom diffuses on an infinite flat surface. It is sometimes called terrace diffusion barrier because a terrace with a big enough surface area can often approximate to an infinite flat surface. The step-edge barrier, also called the Ehrlich–Schwoebel (ES) barrier [1,2], represents the extra energy barrier for an adatom descending over a step edge on a surface. The flat-surface diffusion barrier controls the intralayer mass transport (i.e., within one atomic layer), while the ES barrier controls the interlayer mass transport (i.e., from one atomic layer to another). Furthermore, if a growing three-dimensional (3D) island is faceted with sharp edges (in contrast to "continuous" 3D mound), it has been shown that two forms of adatom diffusion processes may become dominant in controlling the faceted island growth. These are

diffusing over a facet–facet edge [3] or through a facet–step joint [4,5].

In order to obtain diffusion barriers, in principle, the density functional theory (DFT) first-principles method can be used, especially when the size of system to be studied is small enough. However, an experimentally observed Pb mesa often involves more than thousands of atoms [6–14], while it is well-known that the first-principles method is largely limited to where the number of atoms of the system to be calculated is less than ∼500 atoms. From our recent DFT calculations [15], long range interactions have to be considered due to the "liquid-like" behavior of Pb surface. Then, the calculations for barriers, even for the flat-surface diffusion barrier, require the larger supercells. Therefore, it is very difficult to use the DFT method to calculate various other key barriers. This is especially for the step edge, facet–facet edge, or facet–step joint barriers, because one must use a huge supercell (more than ∼1000 atoms) to prevent spurious interactions between adjacent replicas. In this work, we only assume the Pb mesas of interest to be large enough so that the quantum size effect (QSE) is not important, i.e., in the classical growth regime. The second nearest-neighbor modified embedded atom method (2NN MEAM) [16–18], an empirical extension of the modified embedded atom method (MEAM) [19–22], has proved a feasible and effective method in calculating various structures of metals [16–18]. Therefore, we choose

the 2NN MEAM to calculate various possible diffusion paths, and then obtain corresponding diffusion barriers.

In Section 2, we will briefly describe the formalism of the 2NN MEAM. Section 3 will give the details of extensive calculations of diffusion barriers for a Pb adatom (i) on a flat Pb(111) or Pb(001) surface; (ii) crossing a single A- or B-step edge on the Pb(111) surface; (iii) crossing a facet–facet edge between Pb(111) facet and Pb(001) facet, or between Pb(111) facet and Pb(11$\bar{1}$) facet; (iv) crossing a facet–step joint between Pb(001) facet and A-step, or between Pb(11$\bar{1}$) facet and B-step. In these calculations, different diffusion modes are considered: direct hopping of an adatom, and exchange mechanism between an adatom and substrate surface atom(s). In addition, before calculating various diffusion barriers associated with different facets, we will first discuss low-index planes of Pb[$\bar{1}$10] crystallographic zone related to possible choices of sidewalls in the formation of a Pb mesa, and calculate corresponding surface free energies. In Section 4, we make a summary.

2. Theoretical method

The description of the 2NN MEAM has been published [16–18], and in this section, we briefly review this method.

For a unary system, the total energy is approximated as

$$E = \sum_i E_i, \tag{1}$$

where

$$E_i = F(n_i) + \frac{1}{2} \sum_{j(\neq i)} \phi(r_{ij}) \tag{2}$$

is the energy contribution from atom i, and the summation is over all atoms of the system. $F(n_i)$ is the embedding function, n_i is the effective coordination number [22] at atom i, and $\phi(r_{ij})$ is the core–core pair interaction between atoms i and j separated by a distance r_{ij}.

In the initial embedded atom method (EAM) [23], the embedding function is the energy to embed an atom into the background electron sea. The embedding function in the EAM has no analytical form, and generally is obtained by a cubic spline interpolation from experimental data. In the MEAM, $F(n_i)$ is expressed in the analytical form

$$F(n_i) = \alpha E_c \frac{n_i}{Z_1} \ln \frac{n_i}{Z_1}, \tag{3}$$

where α is an adjustable parameter, E_c is the cohesive energy, and Z_1 is the number of nearest neighbors in the perfect bulk crystal. For an fcc structure, $Z_1 = 12$. In this formulation, $F(n_i)$ has no longer the physical meaning in the initial EAM, but the name, the *embedded-atom*, is still retained. Because Eq. (3) is based on the bond-order conservation principle [20,22], $F(n_i)$ can be called the *bond-it order function* [22].

The expression of the effective coordination number n_i is not unique [20,22]. In the present work, we use the form

$$n_i = \frac{2n_{0,i}}{1 + e^{-\Gamma_i}}, \tag{4}$$

where

$$\Gamma_i = \sum_{h=1}^{3} t_h \left(\frac{n_{h,i}}{n_{0,i}} \right)^2 \tag{5}$$

in which t_h are adjustable parameters, the spherical effective coordination number at atom i is

$$n_{0,i} = \sum_{j(\neq i)} m_{0,j}(r_{ij}) \tag{6}$$

and the angular effective coordination numbers at atom i are

$$n_{1,i} = \sqrt{\sum_u \left[\sum_{j(\neq i)} \frac{r_{ij,u}}{r_{ij}} m_{1,j}(r_{ij}) \right]^2}, \tag{7}$$

$$n_{2,i} = \sqrt{\sum_{u,v} \left[\sum_{j(\neq i)} \frac{r_{ij,u} r_{ij,v}}{r_{ij}^2} m_{2,j}(r_{ij}) \right]^2 - \frac{1}{3} \left[\sum_{j(\neq i)} m_{2,j}(r_{ij}) \right]^2} \tag{8}$$

and

$$n_{3,i} = \sqrt{\sum_{u,v,w} \left[\sum_{j(\neq i)} \frac{r_{ij,u} r_{ij,v} r_{ij,w}}{r_{ij}^2} m_{3,j}(r_{ij}) \right]^2 - \frac{3}{5} \sum_u \left[\sum_{j(\neq i)} \frac{r_{ij,u}}{r_{ij}} m_{3,j}(r_{ij}) \right]^2}, \tag{9}$$

where the index u, v, or w denotes the three Cartesian coordinate components: x, y, and z, and any summation about u, v, or w is over all the three components. In Eqs. (6)–(9), the partial effective coordination number $m_{h,j}(r_{ij})$ is the contribution to the effective coordination number n_i from atom j, given by

$$m_{h,j}(r_{ij}) = \exp \left[-\beta_h \left(\frac{r_{ij}}{r_e} - 1 \right) \right], \quad h = 0, 1, 2, \text{ and } 3, \tag{10}$$

where β_h are adjustable parameters, and r_e is the first nearest-neighbor distance in the perfect crystal structure.

The core–core pair interaction between atom i and j is expressed as

$$\phi(r_{ij}) = \psi(r_{ij}) + \sum_{n=1} \left(-\frac{Z_2}{Z_1} S_{ij} \right)^n \psi(\xi^n r_{ij}), \tag{11}$$

where Z_2 is the number of second nearest-neighbor atoms, ξ is the ratio of the second nearest-neighbor distance over the first nearest-neighbor distance in the perfect crystal, S_{ij} is the many body screening function, and the function

$$\psi(r_{ij}) = \frac{2}{Z_1} [E_u(r_{ij}) - F(n_r(r_{ij}))]. \tag{12}$$

In Eq. (12), the universal function

$$E_u(r_{ij}) = -E_c (1 + b + db^3) e^{-b}, \tag{13}$$

where d is an adjustable parameter, and

$$b = \kappa \left(\frac{r_{ij}}{r_e} - 1 \right), \tag{14}$$

with

$$\kappa = \sqrt{\frac{9B\Omega}{E_c}}, \tag{15}$$

where B is the bulk modulus, and Ω is the atomic volume in the perfect crystal. $n_r(r_{ij})$ in Eq. (12) is the reference effective coordination number, and for fcc or bcc structure, it is written as

$$n_r(r_{ij}) = Z_1 m_{0,j}(r_{ij}) + Z_2 S_{ij} m_{0,j}(\xi r_{ij}). \tag{16}$$

The summation in Eq. (11) is performed until the correct value of energy is obtained for the perfect crystal structure. In Eqs. (11) and (16), the many body screening function, S_{ij}, is defined as

$$S_{ij} = \prod_{k \neq i,j} S_{ijk}. \tag{17}$$

Here, the screening factor S_{ijk} is the contribution to S_{ij} from atom k, and expressed as a cutoff function

$$S_{ijk} = f_c \left(\frac{C - C_{\min}}{C_{\max} - C_{\min}} \right), \tag{18}$$

where $C_{\max}$ and $C_{\min}$ are adjustable parameters, and

$$C = \frac{2(W_{ik} + W_{kj}) - (W_{ik} - W_{kj})^2 - 1}{1 - (W_{ik} - W_{kj})^2} \qquad (19)$$

with $W_{ik} = \left(\frac{r_{ik}}{r_{ij}}\right)^2$, and $W_{kj} = \left(\frac{r_{kj}}{r_{ij}}\right)^2$.

The cutoff function satisfies

$$f_c(x) = \begin{cases} 1, & x \geqslant 1, \\ [1 - (1 - x)^4]^2, & 0 < x < 1, \\ 0, & x \leqslant 0. \end{cases} \qquad (20)$$

All parameters in the above equations can be obtained from the appropriate experimental measurements or first-principles calculations. In the present work, our studied system is the Pb mesa, which has an fcc structure. We use the following parameter set [18]: the cohesive energy $E_c = 2.04$ eV, the lattice constant $a = 4.95$ Å, the first nearest-neighbor distance $r_e = a/\sqrt{2} = 3.50$ Å, the bulk modulus $B = 0.488 \times 10^{11}$ N/m^2, $\alpha = 1.01, d = 0.00, \beta_0 = 5.42, \beta_1 = 2.20, \beta_2 = 6.00, \beta_3 = 2.20, t_1 = 3.10, t_2 = 3.91, t_3 = 1.25, C_{max} = 2.08,$ and $C_{min} = 0.81$. Although these potential parameters are obtained by fitting the thermodynamic equilibrium properties, they have been used to calculate not just thermodynamic quantities (e.g., surface energies, and surface relaxations) but also the kinetic quantities (e.g., bulk vacancy migration energy barrier) for Pb, in good agreement with experimental values [18]. In this work, we use these parameters to calculate various surface diffusion barriers, and show that these parameters are still reasonable.

3. Computational details, results and discussion

3.1. Low-index planes of Pb[$\bar{1}10$] zone and their surface free energies

To calculate various diffusion barriers in the growth of a mesa, it is necessary to first study its crystalline facets. In experiments, the growth of Pb on Si(111) [6–14,24–33] or Ge(111) [32,34] has been demonstrated to be via Stranski–Krastanow (SK) mode [35,36], in which 3D Pb islands (or mesas) are formed on a Pb wetting layer. At the temperature around ~200–300 K, a Pb mesa can adopt the equilibrium hexagonal pyramidal shape with a flat top. The flat-top surface has been shown to be (111) atomic plane [6,37] because of its lowest surface free energy.

Based on our calculations of surface free energies, as discussed below, the six sidewalls of a faceted Pb mesa are deduced to be $(11\bar{1}), (010), (\bar{1}11), (001), (1\bar{1}1)$ and (100). This deduction is in
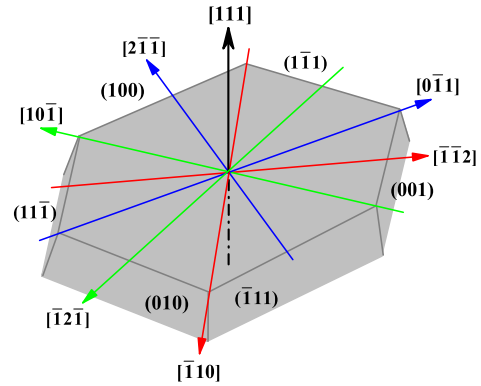

Fig. 1. A schematic faceted fcc mesa with the [111] direction as a symmetry axis. The six sidewalls of the mesa are $(11\bar{1}), (010), (\bar{1}11), (001), (1\bar{1}1)$, and (100) in succession. The threefold symmetry of the crystalline planes and orientations are indicated.

agreement with the experimental observation of Pb(111) mesas grown on Ru(001) substrate [38], but for the case of Pb mesa growth on Si(111) substrate, it still needs to be further confirmed by experimental measurements [39]. Fig. 1 shows the threefold symmetry of the crystal planes and orientations in a faceted fcc mesa with the [111] direction as a symmetry axis. Therefore, consideration of only one of three crystalline zones, $[\bar{1}10], [0\bar{1}1]$ and $[10\bar{1}]$, is needed, and we choose the $[\bar{1}10]$ zone in the discussion below. Fig. 2 shows the low-index planes of this fcc $[\bar{1}10]$ crystalline zone.

In calculating the surface free energy for a flat surface, we use the supercell technique, in which the supercell slab is chosen to be thick enough so that the QSE can be neglected. All atoms in the supercell are relaxed. The surface free energy is given by

$$\gamma = \frac{E - (-NE_c)}{2A}, \qquad (21)$$

where E is the calculated total energy of the supercell, N is the total number of atoms, E_c is the cohesive energy, and A is the area of the top and bottom surface. We first discuss Pb(111) surface, as shown in Fig. 3. Beyond six Pb(111) monolayers thick, the surface free energy from the 2NN MEAM quickly converges to a constant value of 22.57 meV/Å^2. Thus, in the 2NN MEAM calculations of this work, we always choose the thickness of a slab to be more than six Pb(111)
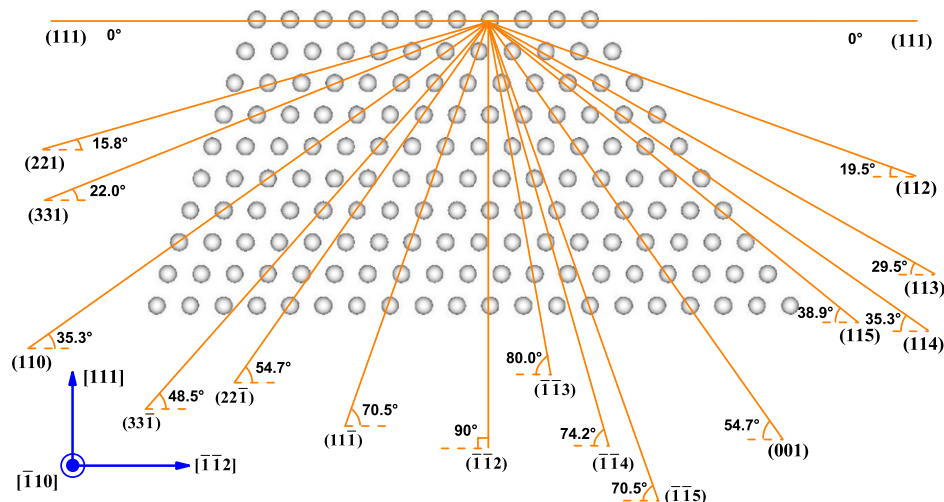

Fig. 2. The low-index planes of fcc $[\bar{1}10]$ crystalline zone. The included angle between each plane and (111) plane are labelled. Note that the mirror symmetry of a crystal plane family, e.g., (221) and (22$\bar{1}$) with respect to (110); ($\bar{1}\bar{1}2$) and (112) with respect to (001); etc.
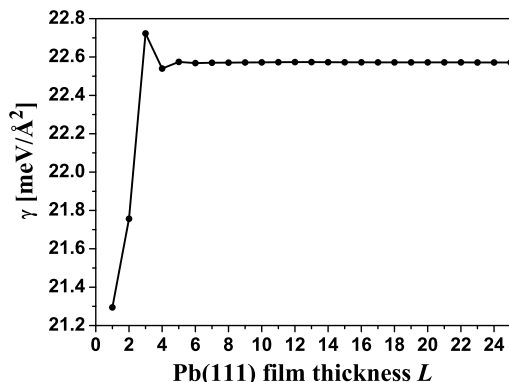
Fig. 3. The Pb(1 1 1) surface free energies of 1–25 ML Pb slabs from the 2NN MEAM calculations.

Fig. 4. The calculated and experimental [38] surface free energies corresponding to the planes shown in Fig. 2 and Table 1. θ is the included angle between each plane and the (1 1 1) plane.

monolayers, representing the classical limit without the influence of QSE.

The calculated (at 0 K) and experimental (at 323 K) [38] surface free energies of low-index planes of Pb[$\bar{1}$10] crystalline zone are listed in Table 1, where the results of first-principles calculations are from previous work [40–42]. Apparently, the (1 1 1) facet has the lowest surface free energy from all calculations and experiments, supporting the observed flat top of Pb mesa to adopt a (1 1 1) top facet. Overall, for all the facets of different orientations, the surface free energies from the 2NN MEAM (at 0 K) are ~4–5 meV/Å^2 higher than the experimental values at 323 K. Fig. 4 shows the plots of surface free energy, γ, vs. the included angle, θ, between a certain plane and the (1 1 1) plane. The surface free energies from the 2NN MEAM are in good overall agreement with experiments [38] for the γ–θ plot, as shown in Fig. 4.

For analyzing the sidewalls of a faceted Pb mesa, we make a vertical cross section (Fig. 2) of the mesa along the [1 1 1] orientation. From Fig. 2, the ($\bar{1}\bar{1}$2) plane is perpendicular to the (1 1 1) plane, and therefore the possible left sidewalls can be ($\bar{1}\bar{1}$2), (11$\bar{1}$), (22$\bar{1}$), (33$\bar{1}$), (110), (331), (221),..., and the possible right sidewalls can be ($\bar{1}\bar{1}$2), ($\bar{1}\bar{1}$3), ($\bar{1}\bar{1}$4), ($\bar{1}\bar{1}$5), (115), (114), (113), (112),... Apparently, the most possible left sidewall should be the (11$\bar{1}$) plane due to its lowest surface free energy. Now, let us look at the right sidewall. From Table 1 and Fig. 4, the surface free energy of the (0 0 1) facet is lowest in the possible right sidewalls, so the most possible right sidewall should adopt a (0 0 1) plane. A vertical facet with the ($\bar{1}\bar{1}$2) plane does not have the lowest surface free energy for either the left side or the right side, and hence it should not be a sidewall, as observed in scanning tunneling microscopy (STM) images [6,7,11,38]. Fig. 1 schematically shows the threefold symmetry of most possible mesa sidewalls and crystalline orientations, according to the above surface free energy criterion.

Furthermore, from Table 1 and Fig. 4, we also note that for the left side, the (2 2 1) facet has the second lowest surface free energy,
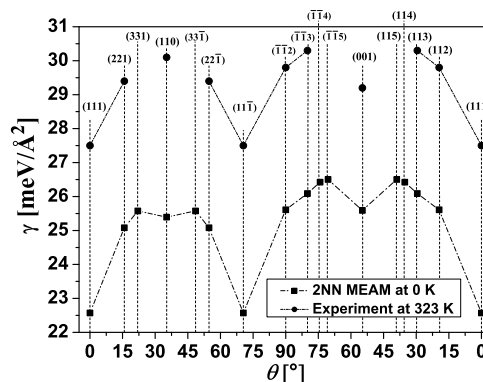
and for the right side, the (1 1 2) facet has the second lowest surface free energy. Therefore, a (2 2 1) facet as a left sidewall will be secondly favorable after the (11$\bar{1}$) facet, and a (1 1 2) facet as a right sidewall will be secondly favorable after the (0 0 1) facet. In the experiments of depositing Pb on Ru(0 0 1) substrate [38], the small (2 2 1) facet has been observed between the top facet (1 1 1) and the sidewall facet (11$\bar{1}$), and the small (1 1 2) facet has been observed between the top facet (1 1 1) and the sidewall facet (0 0 1). However, in the experiments of depositing Pb on Si(1 1 1) substrate, up to now there have not yet been any reports about the sidewall details. In this work, we assume that the six sidewalls of a faceted Pb mesa grown on Si(1 1 1) substrate are (11$\bar{1}$), (0 1 0), ($\bar{1}$1 1), (0 0 1), (1 1$\bar{1}$), and (1 0 0) facets, respectively.

3.2. Diffusion of an adatom on a flat surface

The diffusion barrier is calculated as the energy difference between energy minimum and saddle point on MEP. To obtain the MEP, the nudged elastic band (NEB) method [43], as well as the climbing NEB method (a development of NEB method) [44], can be often used when the studied system has a bad symmetric feature or a relatively high accuracy is required, but it needs to take many enough images in the calculation, and therefore the NEB method could be not efficient, especially for a relatively large system. Another way to be frequently used is the constrained relaxation, in which one or two certain direction(s) (e.g., X- or/and Y-axis) of the adatom is(are) appropriately fixed in terms of the symmetry of the studied surface structure, and other direction(s) of the adatom is(are) allowed to relax. This constrained relaxation method can be more efficient than the NEB method if the symmetric feature of the studied system has already been largely clear. In this work, we choose the constrained relaxation method, and all the atoms in the supercell are relaxed except that the X- and Y-coordinates of the adatom are fixed (i.e., these two coordinates of the

Table 1
A comparison of the surface free energies of low-index planes of Pb[$\bar{1}$10] crystalline zone among the 2NN MEAM, first-principles calculations, and experiments

Method	(1 1 1) (11$\bar{1}$)	(2 2 1) (22$\bar{1}$)	(3 3 1) (33$\bar{1}$)	(1 1 0)	(0 0 1)	($\bar{1}\bar{1}$2) (1 1 2)	($\bar{1}\bar{1}$3) (1 1 3)	($\bar{1}\bar{1}$4) (1 1 4)	($\bar{1}\bar{1}$5) (1 1 5)
(a)	22.57	25.08	25.58	25.39	25.59	25.61	26.09	26.42	26.50
(b)	26.0	–	–	30.8	29.9	–	–	–	–
(c)	17.2	–	–	20.8	20.0	–	–	–	–
(d)	17	–	–	–	–	–	–	–	–
(e)	16.8	–	–	–	–	–	–	–	–
(f)	27.5	29.4	–	30.1	29.2	29.8	30.3	–	–

(a) 2NN MEAM (this work); (b) PPW, LDA-PZ, NLCC [40]; (c) PPW, LDA-PBE, NLCC [40]; (d) UPPW, GGA-PW91 [41]; (e) UPPW, GGA-PW91 5d [42]; (f) experiment at 323 K [38]. The units are in meV/Å^2.

adatom are constrained during the energy minimization). Also, in our calculations of searching the MEP, we always take the output from the current calculated state as the input of the next state to be calculated, and simultaneously make an artificial push against the adatom by a reasonably small displacement along the assumed diffusion path to simulate the "realistic" diffusion process. In principle, the more the calculated states along the path, the closer the simulated results to the "realistic" diffusion path. However, considering the efficiency of simulation, we always limit ourselves to calculate as few as possible states (but make sure the number of calculated states is sufficient, esp. in the region near a saddle point) along the path by firstly doing some necessary tests before the calculation.

In the flat-surface diffusion barrier calculation, a too small supercell will result in a noticeable interaction between adjacent replicas. To avoid this spurious interaction, we always use a big enough supercell with the periodic boundary conditions along X- and Y-axes. Z-axis is perpendicular to the free top and bottom surfaces. We only calculate the diffusion barriers on (1 1 1) and (0 0 1) surfaces because they are most favorable as the Pb mesa top or sidewalls, as discussed in Section 3.1.

For Pb(1 1 1) surface, Fig. 5 shows three assumed diffusion paths of a Pb adatom by direct hopping, and the energies of nine successional states along each diffusion path are calculated. From the fcc site P to its nearest fcc site Q, the energetically most favorable path (i.e., the MEP) is P–M–Q, in which the adatom first hops over one bridge site, and then goes through the hcp site M and again another bridge site toward the fcc site Q. The saddle point is approximately
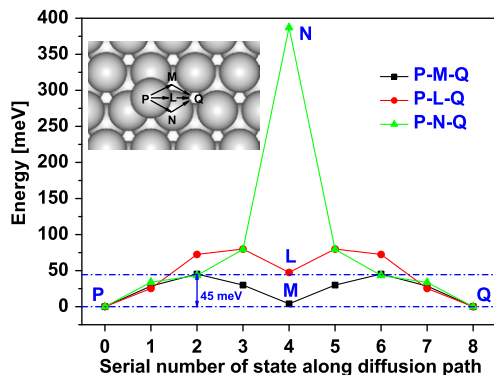
located at the bridge site, and ∼45 meV higher than the energy minimum (on P or Q), as shown in Fig. 5. This barrier value of ∼45 meV is in qualitative agreement with our recent DFT calculations [15]. We also tried to calculate the diffusion barriers of different multi-atom exchange modes [45–47] for flat Pb(1 1 1) surface, and found that these barriers are always much larger than 45 meV. This indicates that direct hopping mode is much more favorable than exchange mechanism for the diffusion of a Pb adatom on flat Pb(1 1 1) surface.

For some fcc metals, when an adatom diffuses on (0 0 1) surface, a two-atom exchange mechanism [45] is often found to be favored over direct hopping mode. For example, the two-atom exchange mechanism has been observed experimentally by using the field ion microscope technology for Ir/Ir(0 0 1) [48], Pt/Pt(0 0 1) [49] and Ni/Pt(0 0 1) [50]. Theoretically, Al/Al(0 0 1) (first-principles) [45], Pt/Pt(0 0 1) (EAM) [51], Au/Au(0 0 1) (EAM) [51], Au/Au(0 0 1) (first-principles) [52], and Pd/Pd(0 0 1) (EAM) [51] also favor this mechanism. However, some cases, e.g., experimentally Rh/Rh(0 0 1) [53], Pd/Pt(0 0 1) [50] and theoretically Cu/Cu(0 0 1) (EAM) [46] favor the direct hopping mode. For Pb/Pb(0 0 1), we also calculate two diffusion modes, as shown in Fig. 6. The obtained diffusion barrier for direct hopping is ∼321 meV, and the diffusion barrier for the two-atom exchange mechanism is ∼404 meV. This indicates that the direct hopping diffusion is favored over the exchange mechanism for the diffusion of a Pb adatom on flat Pb(0 0 1) surface.
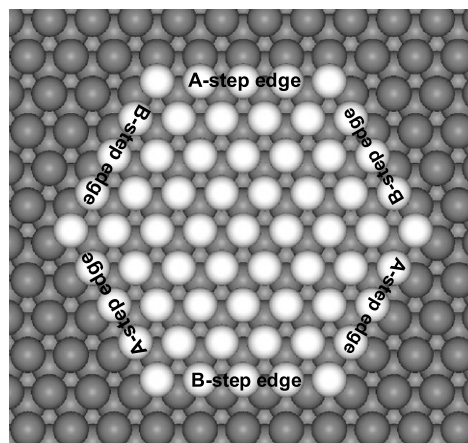

Fig. 5. Three assumed diffusion paths of a Pb adatom by direct hopping on flat Pb(1 1 1) surface. The inset is a top view indicating the diffusion paths of the adatom.

Fig. 7. A monolayer hexagonal adatom island (light color) formed on an fcc (1 1 1) surface indicates two different step types, A- and B-steps, corresponding to their different geometries.
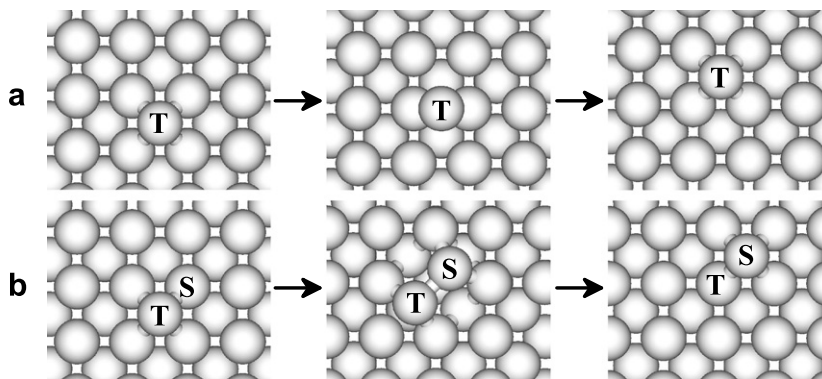

Fig. 6. Two diffusion modes of a Pb adatom on a flat Pb(0 0 1) surface (top views). (a) Direct hopping: the adatom T hops over a bridge site from one hollow site to another neighboring hollow site. (b) Exchange mechanism: the adatom T migrates towards a substrate surface atom S and pushes it out of its site, and then fills the vacant place that the atom S leaves behind. Consequently, the atom S becomes a new adatom, and the previous adatom T becomes a substrate surface atom.
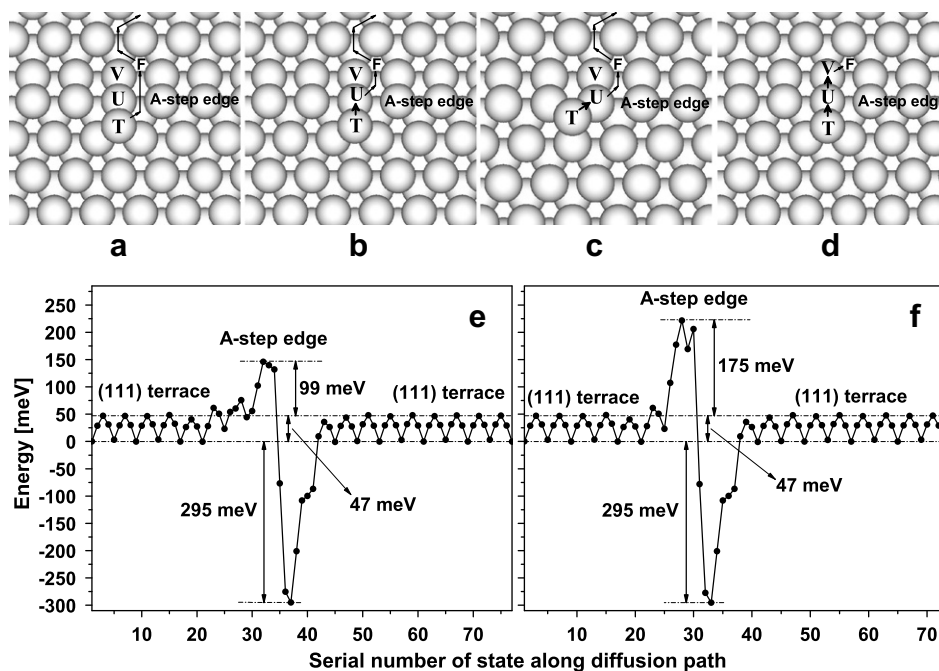
Fig. 8. Four possible diffusion modes of a Pb adatom crossing A-step edge on Pb(1 1 1) surface (top views): (a) direct hopping; (b) Exchange 1; (c) Exchange 2; (d) Exchange 3. For details, see the text. (e) and (f) are energy curves corresponding to (a) and (b), respectively.

3.3. Diffusion of an adatom crossing a single step edge

There are two types of steps, A- and B-steps [54], on the (1 1 1) surface of an fcc structure, as shown in Fig. 7. A- and B-steps correspond to different geometries, so we must separately calculate the diffusion barrier of an adatom crossing a single A- or B-step edge.

For crossing A-step edge, we calculate four possible diffusion modes. Fig. 8a shows the most possible direct hopping mode, in which the adatom T diffuses towards the A-step, and directly hops over the step edge from step top to step bottom, as indicated by the arrows. Fig. 8b shows the first possible exchange mode (labelled as Exchange 1). When the adatom T arrives at the step-top fcc site, it pushes the edge atom U out of its site, and then fills the place that the atom U leaves behind. Consequently, the atom U becomes a new adatom migrating towards the step-bottom fcc site F, as indicated by the arrows. Fig. 8c shows the second possible exchange mode (labelled as Exchange 2), which is similar to Exchange 1, but the adatom T first arrives at the step-top hcp site, and then pushes the edge atom U. Fig. 8d shows the third possible exchange mode (labelled as Exchange 3), which is a three-atom exchange mechanism. When the adatom T arrives at the step-top fcc site, it pushes the edge atom U, and the atom U pushes the bottom atom V. Consequently, the atom V becomes a new adatom migrating towards the step-bottom fcc site F, as indicated by the arrow, while the place of the atom U is replaced with the atom T, and the place of the atom V is replaced with the atom U.

The energy curves corresponding to the direct hopping (Fig. 8a) and Exchange 1 (Fig. 8b) are shown in Fig. 8e and f, respectively. From Fig. 8e and f, the direct hopping with an ES barrier of 99 meV is more favorable than Exchange 1 with an ES barrier of 175 meV. Exchange 2 has an ES barrier of 185 meV (not shown in Fig. 8), and therefore also unfavorable. For Exchange 3, our calculation shows that this three-atom concerted motion has an ES barrier of much larger than 185 meV, and consequently is extremely unfavorable. From Fig. 8e and f, we also note that when an adatom is down to the A-step kink site F (see Fig. 8) from the terrace mini-mum energy adsorption sites, there is a big energy drop of 295 meV. Therefore, the A-step kink site F is just like a "perfect sink", which can easily attach an adatom, but it is difficult to detach the adatom from the sink.

Here, it should be mentioned that when the adatom is far from the step (see Fig. 8e and f), we obtain a terrace diffusion barrier of ∼47 meV, which is a little bit different from the flat-surface value of 45 meV (see Section 3.2). This indicates that for two differently chosen supercell slabs, there is an error bar with an order of a few meV. We find that the largest error is ±9 meV in all of our diffusion barrier calculations of this work.

For crossing B-step edge, we calculate three possible diffusion modes. Fig. 9a shows the most possible direct hopping mode, in which the adatom T diffuses towards the B-step, and directly hops over the step edge from step top to step bottom, as indicated by the arrow. Fig. 9b shows the first possible exchange mode (labelled as Exchange 1). When the adatom T arrives at the step-top hcp site, it pushes the edge atom U out of its site, and then fills the place that the atom U leaves behind. Consequently, the atom U becomes a new adatom migrating towards the step-bottom fcc site F, as indicated by the arrow. Fig. 9c shows the second possible exchange mode (labelled as Exchange 2), which is similar to Exchange 1, but the adatom T first arrives at the step-top fcc site, and then pushes the edge atom U.

The energy curves corresponding to the direct hopping (Fig. 9a) and Exchange 1 (Fig. 9b) are shown in Fig. 9d and e, respectively. From Fig. 9d and e, Exchange 1 with an ES barrier of 31 meV is more favorable than the direct hopping with an ES barrier of 106 meV. Exchange 2 has an ES barrier of a 33 meV (not shown in Fig. 9) very close to that of Exchange 1, and therefore also favorable. From Fig. 9d and e, we again note that when an adatom is down to the B-step kink site F (see Fig. 9) from the terrace mini-mum energy adsorption sites, the energy has a big drop of 277 meV. Therefore, the B-step kink site F is also like a "perfect sink", which is analogous to that of A-step case.

In experiments, an adatom island and then a vacancy island can be formed on the Pb mesa top by the Coulomb sink charging effect
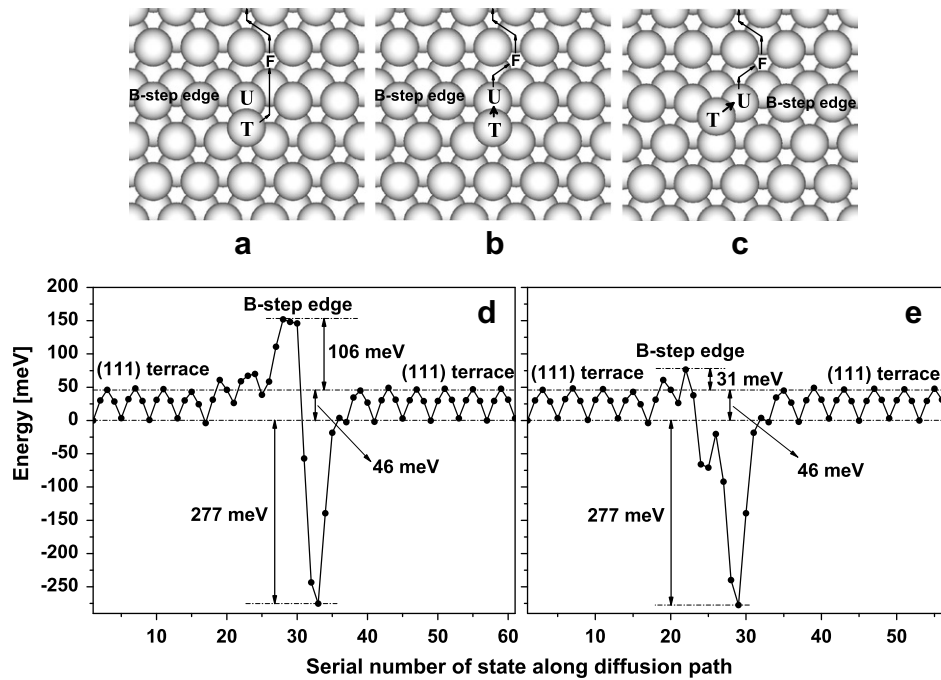
Fig. 9. Three possible diffusion modes of a Pb adatom crossing the B-step edge on the Pb(1 1 1) surface (top views): (a) direct hopping; (b) Exchange 1; (c) Exchange 2. For details, see the text. (d) and (e) are energy curves corresponding to (a) and (b), respectively.

[7,10,11,13,14]. Recently, using the isotropic surface steady-state diffusion equation, we have obtained an "effective" ES barrier of ∼ 83 ± 10 meV at the growth temperature of 300 K, by fitting decay rate of the vacancy island and the growth rate of the adatom island from experiments [10]. Considering average effect of crossing A- and B-step edges, the average value, 65 meV, of the A- and B-step edge barriers (99 meV and 31 meV, respectively) from the present 2NN MEAM calculations agrees well with the above ES barrier fitted from the experimental measurements.
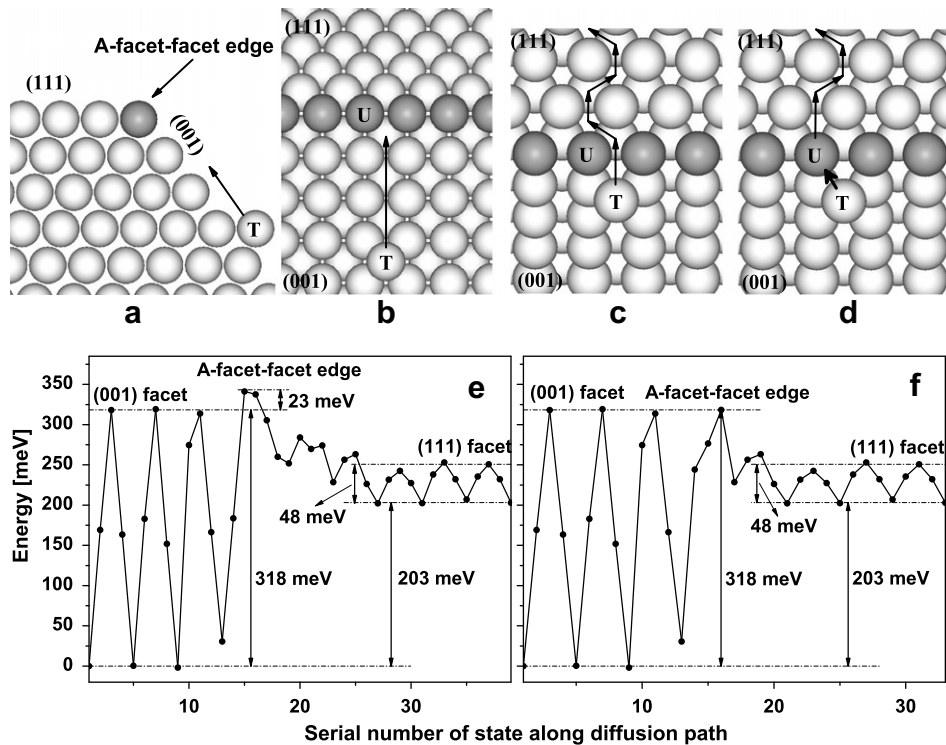

Fig. 10. Two most possible diffusion modes of a Pb adatom crossing the A-facet–facet edge from Pb(0 0 1) facet to Pb(1 1 1) facet: (a) A side view; (b) A (0 0 1)-top view; (c) A (1 1 1)-top view of the direct hopping; (d) A (1 1 1)-top view of the exchange mechanism. For clarity, the A-facet–facet edge is painted with heavy gray. For more explanations, see the text; (e) and (f) are energy curves corresponding to (c) and (d), respectively.

3.4. Diffusion of an adatom crossing a facet–facet edge

In Section 3.1, it has been discussed that in terms of surface free energy, the most favorable right sidewall of a Pb mesa is (001) facet, and the most favorable left sidewall is (11$\bar{1}$) facet, as shown in Fig. 2. Thus, we just calculate the diffusion barrier of an adatom crossing the facet–facet edge from the right sidewall (001) facet to top (111) facet, or from the left sidewall (11$\bar{1}$) facet to top (111) facet.

For the convenience of discussion, we name the adatom diffusion between (001) facet and (111) facet as "A-facet–facet" diffusion, and name the adatom diffusion between (11$\bar{1}$) facet and (111) facet as "B-facet–facet" diffusion. Here, it should be mentioned as a computational detail that because the A- or B-facet–facet diffusion involves the adatom motion from one facet to another facet, we always, by an appropriate coordinate rotation, make the Z-axis perpendicular to the facet that the adatom is diffusing on.

We calculate two most possible diffusion modes for a Pb adatom crossing the A-facet–facet edge from Pb(001) facet to Pb(111) facet. Fig. 10a is a side view, in which the diffusion of adatom T on the (001) facet towards the edge. The arrows denote the diffusion direction. Fig. 10b is a (001)-top view, in which the adatom T first diffuses on the (001) facet towards the edge, and arrives at a hollow site near the edge. Both Fig. 10c and d are the (111)-top views. Fig. 10c shows the most possible direct hopping mode, in which the adatom T directly hops over the edge. The arrows denote the diffusion path. Fig. 10d shows the most possible exchange mechanism, in which the adatom T pushes the edge atom U out of its site, as indicated by the short-thick arrow, and then fills the place that the atom U leaves behind. Consequently, the atom U becomes a new adatom on the (111) facet.

The energy curves corresponding to the direct hopping (Fig. 10c) and the exchange mechanism (Fig. 10d) are shown in Fig. 10e and f, respectively. From Fig. 10e and f, the direct hopping has a small extra barrier of 23 meV, while the exchange mechanism has no extra barrier. Therefore, the exchange mechanism is slightly more favorable than the direct hopping mode.

We calculate four possible diffusion modes for a Pb adatom crossing the B-facet–facet edge from Pb(11$\bar{1}$) facet to Pb(111) facet. Fig. 11a is a side view, in which the diffusion of adatom T on the (11$\bar{1}$) facet towards the edge. The arrows denote the diffusion direction. Fig. 11b is a (11$\bar{1}$)-top view, in which the adatom T first diffuses on the (11$\bar{1}$) facet towards the edge, and arrives at an hcp site H or further an fcc site F near the edge. Figs. 11c–f are all the (111)-top views. Fig. 11c shows the most possible direct hopping mode, in which when the adatom T arrives at the fcc site F, and then directly hops over the edge. The arrows denote the diffusion path. Fig. 11d shows the first possible exchange mode (labelled as Exchange 1), in which when the adatom T arrives at the hcp site H, it pushes the edge atom U out of its site, as indicated by the short-thick arrow, and then fills the place that the atom U leaves behind. Consequently, the atom U becomes a new adatom diffusing
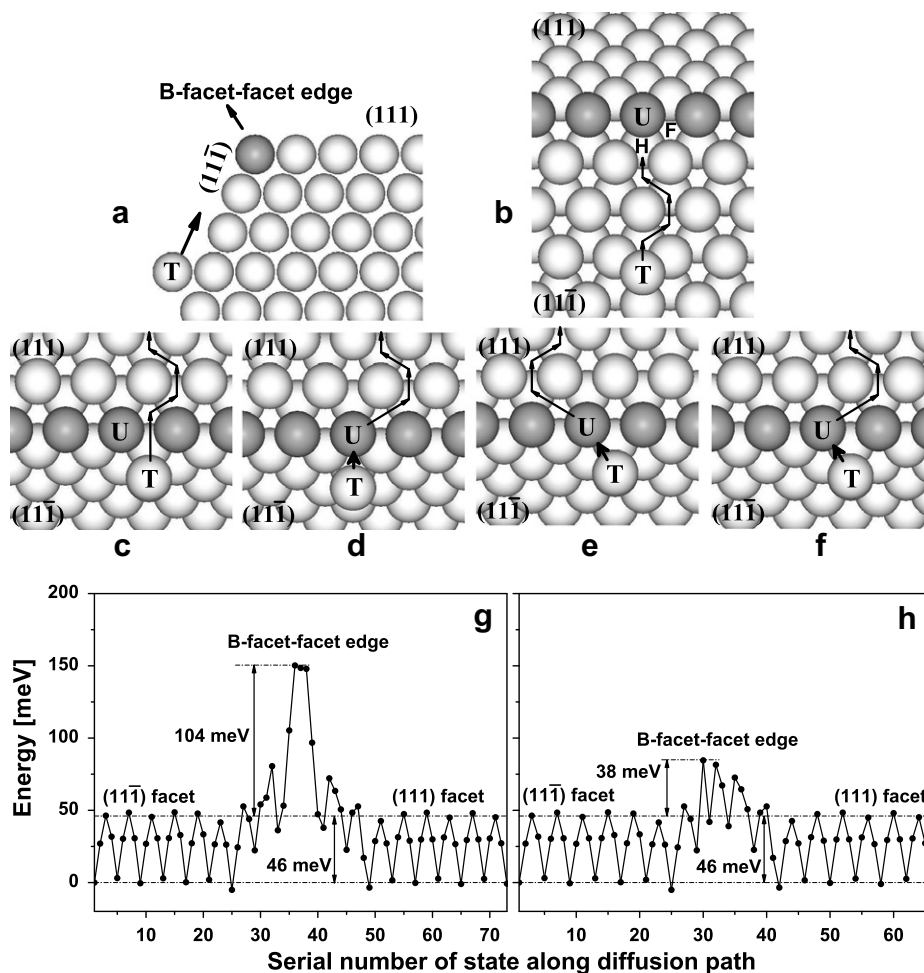

Fig. 11. Four possible diffusion modes of a Pb adatom crossing the B-facet–facet edge from Pb(11$\bar{1}$) facet to Pb(111) facet: (a) A side view; (b) A (11$\bar{1}$)-top view; (c) Direct hopping; (d) Exchange 1; (e) Exchange 2; (f) Exchange 3. For clarity, the B-facet–facet edge is painted with heavy gray. (c)–(f) are all (111)-top views. For more explanations, see the text. (g) and (h) are energy curves corresponding to (c) and (d), respectively.

along the arrows. Fig. 11e shows the second possible exchange mode (labelled as Exchange 2), which is similar to Exchange 1, but the adatom T first arrives at the fcc site F, and then pushes the edge atom U towards the left side along the arrows. Fig. 11f shows the third possible exchange mode (labelled as Exchange 3), which is nearly the same as Exchange 2, but the edge atom U is pushed towards the right side along the arrows.

The energy curves corresponding to the direct hopping (Fig. 11c) and the exchange mechanism (Fig. 11d) are shown in Fig. 11g and h, respectively. From Fig. 11g and h, the direct hopping has a larger extra barrier of 104 meV, and Exchange 1 has a relatively smaller extra barrier of 38 meV, while both Exchange 2 and Exchange 3 have the larger extra barriers of $\sim$ 115 meV (not shown in Fig. 11). Therefore, Exchange 1 is the most favorable one among the four calculated diffusion modes.

From Fig. 10e and f, we note that if an adatom climbs up to the minimum energy adsorption site of (1 1 1) facet from the minimum energy adsorption site of (0 0 1) facet (also see Fig. 10), the energy of system will have to increase by at least $\sim$ 203 meV. This large energy increase implies that the A-facet–facet diffusion from (0 0 1) facet to (1 1 1) facet is extremely unfavorable in spite of the zero extra barrier. Thus, the adatom is thermodynamically prevented from climbing onto (1 1 1) facet from (0 0 1) facet. Also, (1 1 $\bar{1}$) facet and (1 1 1) facet belong to the same family {1 1 1}, so that they have the same adsorption energy, as shown in Fig. 11g and h. However, Fig. 11h shows that there is an additional 38 meV energy barrier for an adatom to cross the B-facet–facet edge from (1 1 $\bar{1}$) facet to (1 1 1) facet. Thus, the adatom is kinetically hindered from climbing onto (1 1 1) facet from (1 1 $\bar{1}$) facet.

The above results indicate that, normally, the adatom concentration must be very low on the mesa top {1 1 1} facet, because it is difficult for adatoms to climb onto the mesa top either thermodynamically from the {0 0 1} sidewalls or kinetically from the {1 1 1} sidewalls. This is consistent with the experimental observation that flat-top Pb(1 1 1) mesas are extremely stable staying in-tact for days, and the island nucleation and overgrowth on the mesa top can only be triggered by an external perturbation using STM pulse [6].

3.5. Diffusion of an adatom crossing a facet–step joint

When an adatom climbs up from a sidewall {0 0 1} or {1 1 1} facet to a step kink site on the mesa top {1 1 1}, it may go through four possible types of facet–step joints, which are denoted as AA joint (from {0 0 1} facet to A-step), AB joint (from {0 0 1} facet to B-step), BA joint (from {1 1 1} facet to A-step), and BB joint (from {1 1 1} facet to B-step), respectively. From all our calculations, it is known that when an adatom crosses all these four possible facet–step (AA, AB, BA, and BB) joints, the energy curves for adatom diffusion are similar. Below, we only illustrate two typical diffusions for the cases of crossing AA and BB joints.

As the computational details, here we need to mention that by doing tests, in our above flat-surface diffusion barrier calculations, the supercell can be relatively small ($\sim$100 atoms) with the periodic boundary conditions along two directions (X- and Y-axes); for the step-edge diffusion barrier calculations, to avoid not only the spurious adatom–adatom interaction but also the spurious step-step interaction between the adjacent replicas, we take the supercell to be relatively bigger (more than $\sim$1000 atoms); for the facet–facet diffusion barrier calculations, to make the terraces wide enough with the periodic boundary condition along only one direction (X-axis), the supercell is also chosen to be relatively bigger (more than $\sim$1000 atoms). In the following facet–step diffusion barrier calculations, there is no periodicity available in all three directions (X-, Y-, and Z-axes) due to the complicacy of the studied system, so that we have to use a much larger supercell (more than $\sim$1500 atoms). In addition, similar to the calculations for facet–facet edge barriers in Section 3.4, we always, by an appropriate coordinate rotation, make the Z-axis perpendicular to the facet that the adatom is diffusing on.
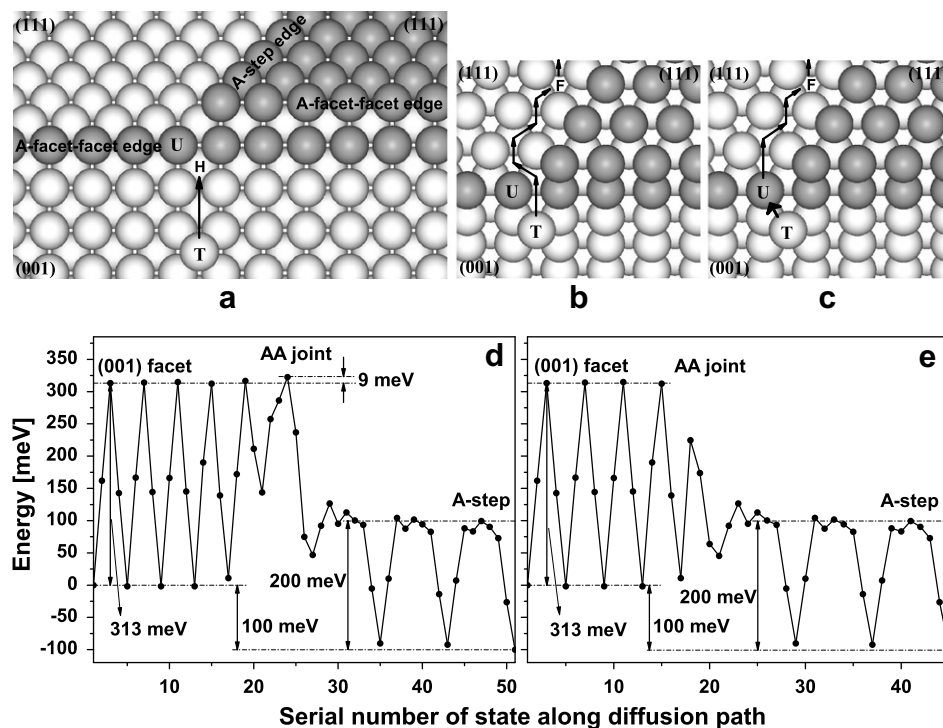

Fig. 12. Two most possible diffusion modes of a Pb adatom crossing the AA joint from Pb(0 0 1) facet to A-step: (a) A (0 0 1)-top view; (b) A (1 1 1)-top view of the direct hopping mode; (c) A (1 1 1)-top view of the exchange mode. For clarity, the monolayer Pb island on Pb(1 1 1) and the A-facet–facet edge are painted with heavy gray. For more explanations, see the text. (d) and (e) are energy curves corresponding to (b) and (c), respectively.
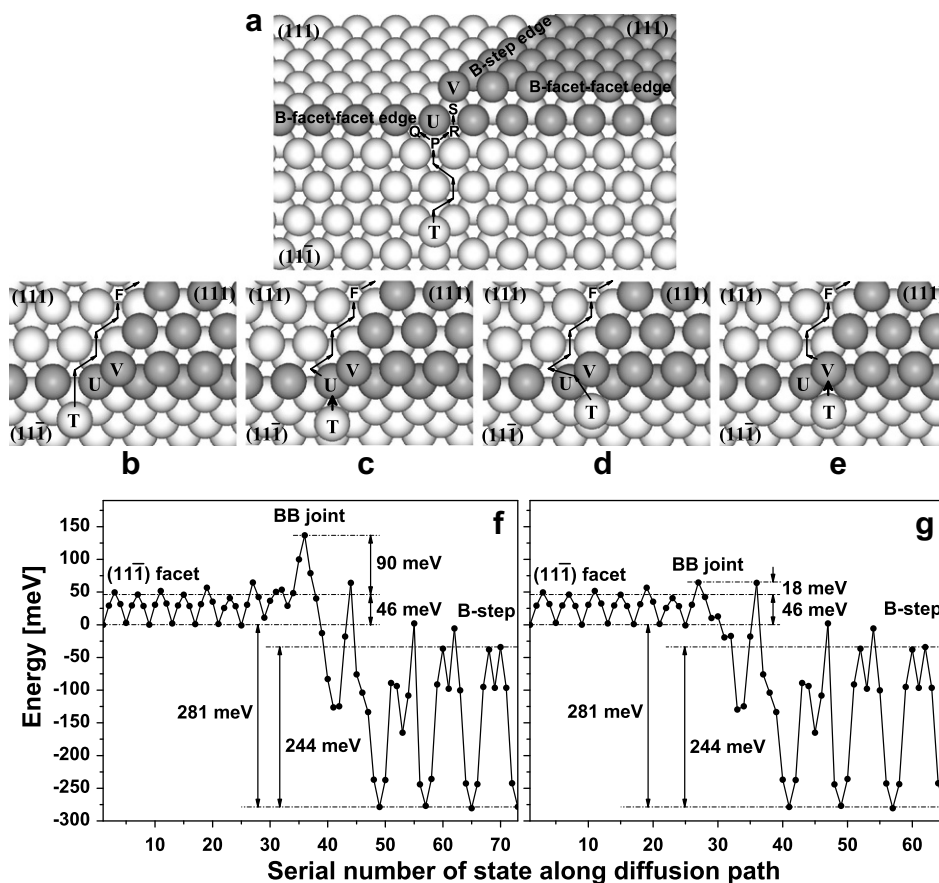
Fig. 13. Four possible diffusion modes of a Pb adatom T crossing the B-facet–step joint from Pb(11$\bar{1}$) facet to B-step: (a) A (11$\bar{1}$)-top view; (b) Hopping 1; (c) Exchange 1; (d) Hopping 2; (e) Exchange 2. (b)–(e) are (111)-top views. For clarity, the single-layer Pb island on Pb(111) and the B-facet–facet edges are painted with heavy gray. For more explanations, see the text. (f) and (g) are energy curves corresponding to (b) and (c), respectively.

In Fig. 12, we show two most possible diffusion modes of a Pb adatom crossing the AA joint from Pb(001) facet to A-step. Fig. 12a is a (001)-top view, in which the adatom T first diffuses on the (001) facet towards the edge, and arrives at a hollow site H near the joint. The arrow denotes the diffusion direction. Both Figs. 12b and c are the (111)-top views. Fig. 12b shows the most possible direct hopping mode, in which the adatom T directly hops over the edge. The arrows denote the diffusion path. Fig. 12c shows the most possible exchange mode, in which the adatom T pushes the edge atom U out of its site, as indicated by the short-thick arrow, and then fills the place that the atom U leaves behind. Consequently, the atom U becomes a new adatom diffusing along the arrows.

The energy curves corresponding to the direct hopping (Fig. 12b) and the exchange mechanism (Fig. 12c) are shown in Fig. 12d and e, respectively. From Fig. 12d and e, the direct hopping has a tiny extra barrier of 9 meV, while the exchange mechanism has no extra barrier. We also note that the minimum adsorption energy has a drop of ∼ 100 meV from (001) facet to (111) facet (Fig. 12d and e). Therefore, the adatom diffusion of crossing the AA joint from (001) facet to A-step will be thermodynamically allowable, in contrast to the case of crossing the A-facet–facet edge (Section 3.4). In addition, from Fig. 12d or e, the adatom diffusion along the A-step edge has a rather large barrier of 200 meV.

Fig. 13 shows the two possible direct hopping modes and two possible exchange modes of a Pb adatom crossing the BB joint from Pb(11$\bar{1}$) facet to B-step. Fig. 13a is a (11$\bar{1}$)-top view, in which the adatom T first diffuses on the (11$\bar{1}$) facet towards the edge, and arrives at the hcp site P near the joint. The arrows denote the diffu-

sion directions. Figs. 12b–e are all the (111)-top views. Fig. 12b shows the first possible direct hopping mode (labelled as Hopping 1), in which, from the site P, the adatom T first arrives at the fcc site Q near the joint, and then directly hops over the A-facet–facet edge. The arrows denote the diffusion path. Fig. 12c shows the first possible exchange mode (labelled as Exchange 1), in which, at the site P, the adatom T pushes the edge atom U out of its site, as indicated by the short-thick arrow, and then fills the place that the atom U leaves behind. Consequently, the atom U becomes a new adatom diffusing along the arrows. Fig. 12d shows the second possible direct hopping mode (labelled as Hopping 2), in which, from the site P, the adatom first arrives at the site S via the site R, and then directly hops over the bridge between atom U and atom V towards the fcc site near the joint. The arrows denote the diffusion path. Fig. 12e shows the second possible exchange mode (labelled as Exchange 2), in which, the adatom T arriving at the site S pushes the edge atom V out of its site, and then fills the place that the atom V leaves behind. Consequently, the atom V becomes a new adatom diffusing along the arrows.

The energy curves corresponding to Hopping 1 (Fig. 13b) and Exchange 1 (Fig. 13c) are shown in Fig. 13f and g, respectively. From Fig. 13f and g, Hopping 1 has a extra barrier of 90 meV, while Exchange 1 has a small extra barrier of 18 meV. Also, Hopping 2 has a extra barrier of 109 meV, while Exchange 2 has a barrier of 51 meV (not shown in Fig. 13). Thus, Exchange 1 is most favorable kinetically. Similar to the case of crossing AA joint from (001) facet to A-step (Fig. 12d and e), the minimum adsorption energy from (11$\bar{1}$) facet to (111) facet (Fig. 13f and g) has a big drop, which is ∼ 281 meV. Therefore, the adatom diffusion of crossing the BB

Table 2
The calculated diffusion barriers of an adatom on a flat surfaces, and the calculated *extra* diffusion barriers of an adatom crossing A- and B-steps, A- and B-facet–facet edges, as well as AA and BB joints (in meV units)

Adatom motion	Direct hopping	Exchange mechanism
On $(1\,1\,1)$	45	$\gg$45
On $(0\,0\,1)$	321	404
Crossing A-step edge	99	175
Crossing B-step edge	106	31
Crossing A-facet–facet edge from $(0\,0\,1)$ to $(1\,1\,1)$	23	0
Crossing B-facet–facet edge from $(1\,1\,\bar{1})$ to $(1\,1\,1)$	104	38
Crossing AA joint from $(0\,0\,1)$ to A-step	9	0
Crossing BB joint from $(1\,1\,\bar{1})$ to B-step	90	18

joint from $(1\,1\,\bar{1})$ facet to A-step will be thermodynamically favorable, in contrast to the case of crossing the B-facet–facet edge (Section 3.4). In addition, from Fig. 13f or g, the adatom diffusion along the B-step edge has a large barrier of 244 meV.

3.6. An explanation for kinetic growth of a Pb mesa in experiments

In recent experiments, an unusual growth behavior of Pb mesa has been observed [6–10,14]. Briefly, Pb mesas are first grown on Si(1 1 1) substrate. Then, nucleation and growth of a 2D island in the middle of mesa top was triggered by applying a STM pulse through the Coulomb sink effect [7,10,11,13,14]. After removing the STM tip from the Pb mesa top, the 2D island continues to grow until a complete overlayer is formed on the top. When the STM tip is quickly removed from the Pb mesa top, the discharging process [13] is so quick that the followed growth behavior of Pb mesa will not be impacted by charge effects. One interesting observation is that the rate of overlayer growth undergoes three different stages: First, the 2D island expands slowly in the middle of the mesa top until it touches the edge of the mesa top. Second, as soon as the island touches the edge, it grows rapidly along the edge to form a closed annular ring around the mesa top. Last, the annular ring grows inward again slowly until it closes to form a complete overlayer. The growth rate of stage 2 is several orders of magnitude higher than that of stages 1 and 3, and the stage 3 is slightly slower than the stage 1. In order to understand this intriguing kinetics of Pb mesa overlayer growth, we have given a plausible explanation by using the energy parameters (especially the various diffusion barriers), which have been obtained in this work. For the details, see our recently published paper [14].

In Table 2, we list the calculated flat-surface, step-edge, facet–facet, and facet–step diffusion barriers. As discussed in the above sections, for either direct hopping or exchange mechanism, the possible diffusion path is not unique. In Table 2, we only list the barrier values corresponding to the *most favorable* direct hopping or exchange diffusion paths.

4. Conclusion

In conclusion, we have made an extensive investigation on the possible diffusion modes of a Pb adatom on a flat surface, as well as crossing step-edge, facet–facet edge, and facet–step joints, using the 2NN MEAM. The adatom diffusion paths and diffusion barriers under various different diffusion modes have been obtained. Our

results can provide a good explanation to understand the unusual kinetic growth behavior of a faceted Pb mesa in the recent experiments, and should be also useful as input to further perform the numerical simulations for the epitaxial growth of a Pb mesa.

References

[1] G. Ehrlich, F.G. Hudda, J. Chem. Phys. 44 (1966) 1039.
[2] R.L. Schwoebel, E.J. Shipsey, J. Appl. Phys. 37 (1966) 3682.
[3] S.J. Liu, H. Huang, C.H. Woo, Appl. Phys. Lett. 80 (2002) 3295.
[4] H. Huang, J. Comput. Aid. Mater. Des. 9 (2002) 75.
[5] H. Huang, J. Wang, Appl. Phys. Lett. 83 (2003) 4752.
[6] C.-S. Jiang et al., Phys. Rev. Lett. 92 (2004) 106104.
[7] Y. Han et al., Phys. Rev. Lett. 93 (2004) 106102.
[8] Z. Kuntova, M. Hupalo, Z. Chvoj, M. Tringides, Surf. Sci. 600 (2006) 4765.
[9] H. Okamoto, D. Chen, T. Yamada, Phys. Rev. Lett. 89 (2002) 256101.
[10] S.-C. Li, Y. Han, J.-F. Jia, Q.-K. Xue, F. Liu, Phys. Rev. B 74 (2006) 195428.
[11] S.-C. Li et al., Appl. Phys. Lett. 89 (2006) 123111.
[12] Y. Han, M. Hupalo, M.C. Tringides, F. Liu, Surf. Sci. 602 (2008) 62.
[13] Y. Han, F. Liu, Front. Phys. China 3 (2008) 41.
[14] Y. Han et al., Appl. Phys. Lett. 92 (2008) 021909.
[15] Y. Han, F. Liu, in preparation.
[16] B.-J. Lee, M.I. Baskes, Phys. Rev. B 62 (2000) 8564.
[17] B.-J. Lee, M. Baskes, H. Kim, Y.K. Cho, Phys. Rev. B 64 (2001) 184102.
[18] B.-J. Lee, J.-H. Shim, M.I. Baskes, Phys. Rev. B 68 (2003) 144112.
[19] M.I. Baskes, Phys. Rev. Lett. 59 (1987) 2666.
[20] M.I. Baskes, J.S. Nelson, A. Wright, Phys. Rev. B 40 (1989) 6085.
[21] M.I. Baskes, Phys. Rev. B 46 (1992) 2727.
[22] P. van Beurden, G.J. Kramer, Phys. Rev. B 63 (2001) 165106.
[23] M.S. Daw, M.I. Baskes, Phys. Rev. B 29 (1984) 6443.
[24] V. Yeh, L. Berbil-Bautista, C.Z. Wang, K.M. Ho, M.C. Tringides, Phys. Rev. Lett. 85 (2000) 5158.
[25] W.B. Su et al., Phys. Rev. Lett. 86 (2001) 5116.
[26] S.H. Chang et al., Phys. Rev. B 65 (2002) 245401.
[27] H. Hong et al., Phys. Rev. Lett. 90 (2003) 076104.
[28] A. Menzel et al., Phys. Rev. B 67 (2003) 165314.
[29] M.H. Upton, C.M. Wei, M.Y. Chou, T. Miller, T.-C. Chiang, Phys. Rev. Lett. 93 (2004) 026802.
[30] P. Czoschke, H. Hong, L. Basile, T.-C. Chiang, Phys. Rev. Lett. 93 (2004) 036103.
[31] Y.-F. Zhang et al., Phys. Rev. Lett. 95 (2005) 096802.
[32] M.M. Özer, Y. Jia, B. Wu, Z. Zhang, H.H. Weitering, Phys. Rev. B 72 (2005) 113409.
[33] Y.-F. Zhang et al., Surf. Sci. 596 (2005) L331.
[34] Y. Jia, B. Wu, H.H. Weitering, Z. Zhang, Phys. Rev. B 74 (2006) 035433.
[35] E. Bauer, Z. Kristallogr. 110 (1958) 372.
[36] F. Liu, Phys. Rev. Lett. 89 (2002) 246105.
[37] M. Jalochowski, E. Bauer, J. Appl. Phys. 63 (1988) 4501.
[38] C. Bombis, A. Emundts, M. Nowicki, H.P. Bonzel, Surf. Sci. 511 (2002) 83.
[39] C.-K Shih, private communication.
[40] D. Yu, M. Scheffler, Phys. Rev. B 70 (2004) 155417.
[41] P.J. Feibelman, Phys. Rev. B 65 (2002) 129902.
[42] C.M. Wei, M.Y. Chou, Phys. Rev. B 66 (2002) 233408.
[43] G. Mills, H. Jónsson, G.K. Schenter, Surf. Sci. 324 (1995) 305.
[44] G. Henkelman, H. Jónsson, J. Chem. Phys. 113 (2000) 9978.
[45] P.J. Feibelman, Phys. Rev. Lett. 65 (1990) 729.
[46] M. Karimi, T. Tomkowski, G. Vidali, O. Biham, Phys. Rev. B 52 (1995) 5364.
[47] G. Henkelman, H. Jónsson, J. Chem. Phys. 111 (1999) 7010.
[48] C. Chen, T.T. Tsong, Phys. Rev. Lett. 64 (1990) 3147.
[49] G.L. Kellogg, P.J. Feibelman, Phys. Rev. Lett. 64 (1990) 3143.
[50] G.L. Kellogg, A.F. Wright, M.S. Daw, J. Vac. Sci. Technol. A 9 (1991) 1757.
[51] C.L. Liu, J.M. Cohen, J.B. Adams, A.F. Voter, Surf. Sci. 253 (1991) 334.
[52] B.D. Yu, M. Scheffler, Phys. Rev. B 56 (1997) R15569.
[53] G. Ayrault, G. Ehrlich, J. Chem. Phys. 60 (1974) 281.
[54] S. Liu, Z. Zhang, G. Comsa, H. Metiu, Phys. Rev. Lett. 71 (1993) 2967.